JOURNAL OF COMPUTATIONAL PHYSICS **147,** 568–593 (1998)
ARTICLE NO. CP986102

Eigenmode Analysis of Unsteady Flows about Airfoils

Răzvan Florea and Kenneth C. Hall

Department of Mechanical Engineering and Materials Science, Duke University, Durham, North Carolina 27708-0300

Received December 16, 1997; revised July 30, 1998

We present a reduced-order modelling technique for analyzing the unsteady subsonic aerodynamic flow about isolated airfoils. To start, we model the flow using the time-linearized full potential equation. The linearized potential equation is discretized on a computational mesh composed of quadrilateral elements using a variational finite element technique. The resulting discretized equations are linear in the unknown potential, but quadratic in the reduced frequency of vibration. We compute the dominant (low frequency) eigenfrequencies and mode shapes of the unsteady fluid motion using a nonsymmetric Lanczos algorithm, and then we use these eigenmodes to construct a low degree-of-freedom reduced-order model of the unsteady flow field. A static correction technique is used to account for the high-frequency eigenmodes not retained in the model. We show that the unsteady flow can be modelled accurately using a relatively small number of eigenmodes. © 1998 Academic Press

1. INTRODUCTION

In this paper, we present a new approach for computing unsteady flows about isolated airfoils. In particular, we first compute the dominant natural frequencies (eigenvalues) and mode shapes (eigenmodes) of unsteady fluid motion about the airfoil. Then, using a small number of these natural modes, we assemble a "reduced-order model" of the unsteady flow field.

Until recently, most unsteady aerodynamic analyses of unsteady flows about wings and airfoils have been one of two types: time domain or frequency domain. In the time-domain approach (see, e.g., [1–6]), one discretizes the fluid equations of motion on a computational grid surrounding the airfoil. The solution is then marched from one time level to the next subject to appropriate unsteady boundary conditions, e.g. arising from the prescribed motion of the airfoil. The advantage of this approach is that it is relatively straightforward to implement and can model nonlinear as well as linear disturbances. However, because of the need for such schemes to be both time accurate and stable, the size of the time step will

0021-9991/98 $25.00
Copyright © 1998 by Academic Press
All rights of reproduction in any form reserved.

generally be quite small, especially for explicit schemes. Furthermore, if the unsteady flow must be calculated for a number of frequencies and mode shapes of airfoil vibration, then a separate time-domain analysis must be performed for each case leading to excessively large computational times.

The other widely used approach is the frequency domain or "time-linearized" technique (see, e.g., [7–13]). Using this approach, one first computes the time-mean (steady) flow about the airfoil by solving the steady flow equations using conventional computational fluid dynamic (CFD) techniques. One then assumes that any unsteadiness in the flow is small and harmonic. The governing fluid equations of motion and the associated boundary conditions are linearized about the mean flow solution to arrive at a set of linear variable coefficient equations that describe the small disturbance flow. The resulting time-linearized equations can be solved very efficiently. Nevertheless, as in the time-domain approach, a separate analysis must be performed for each frequency and vibrational mode shape of interest.

Both the time-domain and frequency domain analyses predict the unsteady flow field for a single prescribed unsteady condition. Thus, other than through extensive parametric studies, these models do not always provide insight into the physics of the unsteady flow. Furthermore, because of the form of these models and the large number of degrees of freedom, the time-domain and frequency-domain models are not well suited for applications involving active control. To reduce the number of degrees of freedom to a manageable level, a number of investigators have developed reduced order models based on curve-fitting techniques (see [14–17]). Usually, the unsteady aerodynamic response (e.g., the unsteady lift due to plunging motion) is fit to a sum of exponentials in time. This form of reduced-order model is especially convenient because the Laplace transform is simply a rational polynomial in the Laplace plane. However, these curve-fit reduced-order models are not completely satisfactory because the time-domain or frequency-domain analyses on which they are based must still be applied at a number of different frequencies. Furthermore, these models make no attempt to use information about the fluid eigenmodes, which presumably play an important role in the fluid motion.

In structural dynamic problems, the conventional approach to solving unsteady vibration problems is to construct reduced-order models using the eigenmodes of the structure as basis functions. It seems plausible that some of the techniques developed for structural dynamic problems could be applied to unsteady aerodynamic flows. In fact, modal analysis techniques have been applied to selected fluid flow problems, for example, boundary layer stability and fluid slosh in tanks. However, only recently have investigators computed the natural frequencies and mode shapes of unsteady flows about airfoils.

Parker [18] has computed the natural frequencies of acoustic modes in a cascade of flat-plate airfoils operating at low Mach numbers. He found his predicted natural frequencies to be in good agreement with experimentally measured values. More recently, Rizzi and Eriksson [19] computed the smallest eigenvalues of a linearized unsteady two-dimensional Euler flow solver. In particular they studied the effect of the far-field boundary conditions and artificial viscosity on the conditioning of the numerical integration scheme. Mahajan, Dowell, and Bliss [20, 21] have computed the eigenfrequencies of viscous flow over isolated airfoils modelled with a Navier–Stokes solver to better understand the role of artificial viscosity. Mahajan, Dowell, and Bliss [22] have also computed the coupled fluid/structure eigenvalues for the case of compressible flow over an elastic airfoil. The present authors have computed the natural frequencies and mode shapes of unsteady compressible cascade flows [23] and incompressible unsteady flows about two-dimensional airfoils, cascades,

and three-dimensional wings ([24]), and have used the resulting eigenvalues to construct low degree-of-freedom reduced-order aerodynamic models. Romanowski and Dowell [25] have used the eigenmodes of a time-domain Euler code to form reduced-order models of flows about isolated airfoils.

Another approach for constructing reduced-order models is based on proper orthogonal decomposition. In this approach one computes the aeroelastic response due to a step in pitch, for example, as a function of time. Then, at several instants in time, one computes the deviation of the unsteady flow field from the mean flow field producing an ensemble of flow field perturbations. The dominant eigenvectors of the autocovariance matrix based on this assemble are used to form a reduced-order aeroelastic model. Note that in both the eigenmode-based and the proper orthogonal decomposition reduced order models, a relatively small dimension basis is extracted from an accurate representation of the unsteady flow. The unsteady aerodynamic/aeroelastic equations are then projected onto the spaced spaned by the basis. Romanowski [26] applied the proper orthogonal decomposition technique to the unsteady aerodynamic flow around a subsonic isolated airfoil described by the Euler equations. A review of this method is provided by Sirovich [27] and by Holmes, Lumley, and Berkooz [28].

In this paper, we apply the concepts developed by Hall, Florea, and Lanzkron [23] to model the unsteady subsonic compressible flow about an isolated airfoil. We show that the unsteady flow can be modelled accurately and efficiently using reduced-order models constructed using a small number of eigenmodes, provided that one or more so-called "static corrections" are applied to approximate the influence of the high-frequency eigenmodes not retained in the model. Work is underway to extend the method to transonic flow using both the full potential equations and the Euler equations. Preliminary results show that no additional difficulties encountered in either the flow model linearization or the eigenvalue calculations.

2. FLOW FIELD DESCRIPTION

2.1. *Nonlinear Full Potential Flow Model*

In this paper, we consider the unsteady subsonic flow about an isolated two-dimensional airfoil due to vibratory motion of the airfoil (the flutter problem). We assume that the flow is isentropic and that any boundary layers are thin and attached. Under these circumstances, the full potential equation provides a reasonably accurate description of the actual flow field. The full potential equation is given by

$$\nabla^2\hat{\phi} = \frac{1}{\hat{c}^2}\left[\frac{\partial^2\hat{\phi}}{\partial t^2} + 2\nabla\hat{\phi}\cdot\frac{\partial\hat{\phi}}{\partial t} + \frac{1}{2}\nabla\hat{\phi}\cdot(\nabla\hat{\phi})^2\right], \tag{1}$$

where $\hat{\phi}$ is the velocity potential and $\hat{c}$ is the local speed of sound. The scalar velocity potential is related to the fluid velocity by $\hat{\mathbf{v}} = \nabla\hat{\phi}$. The superscript "ˆ" indicates that the quantity is unsteady.

The unsteady static pressure $\hat{p}$ and density $\hat{\rho}$ are related to the velocity potential by the unsteady compressible Bernoulli equation,

$$\hat{p} = P_T\left\{1 - \frac{\gamma-1}{C_T^2}\left[\frac{1}{2}(\nabla\hat{\phi})^2 + \frac{\partial\hat{\phi}}{\partial t}\right]\right\}^{\gamma/(\gamma-1)}, \tag{2}$$

where P_T is the total pressure, γ is the ratio of specific heats, and C_T is the total speed of

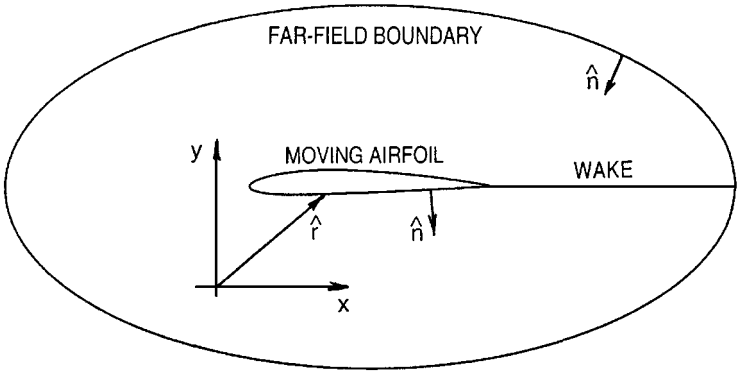

FIG. 1. Domain for the solution of the steady and linearized unsteady full potential equations.

sound. Similarly, the unsteady density is given by

$$\hat{\rho} = \rho_T \left\{ 1 - \frac{\gamma - 1}{C_T^2} \left[\frac{1}{2} (\nabla \hat{\phi})^2 + \frac{\partial \hat{\phi}}{\partial t} \right] \right\}^{1/(\gamma - 1)}, \tag{3}$$

where ρ_T is the total density.

In addition to the governing field equation, boundary conditions are required to complete the problem specification (see Fig. 1). The surface of the airfoil is impermeable. Therefore, the airfoil boundary condition requires that the velocity of the fluid normal to the boundary be equal to the normal component of velocity of the airfoil itself. Hence, we may write

$$\nabla \hat{\phi} \cdot \hat{\mathbf{n}} = \frac{\partial \hat{\mathbf{r}}}{\partial t} \cdot \hat{\mathbf{n}}, \tag{4}$$

where $\hat{\mathbf{r}}(s, t)$ is the prescribed position of a point s on the airfoil as a function of time, and $\hat{\mathbf{n}}$ is the unit normal to the airfoil surface pointing into the fluid.

The unsteady wake shed behind the airfoil is a sheet of vorticity in an otherwise irrotational flow field. In the present work, we model the vortex sheet as a massless impermeable membrane. Because the membrane is impermeable, the boundary condition given in (4) also applies on either side of the wake. However, now the position $\hat{\mathbf{r}}(s, t)$ of a point s on the wake as a function of time is not known *a priori* but, instead, must be found as part of the solution. In addition, since the membrane is massless, it cannot support a pressure jump. Therefore, we require that

$$[\![\hat{p}]\!] = 0, \tag{5}$$

where $[\![\hat{p}]\!]$ is the pressure jump across the wake. Finally, the Kutta condition is applied by requiring that the wake remain attached to the trailing edge of the the airfoil.

In addition to the near-field boundary conditions, far-field boundary conditions must be applied to ensure that the mean flow velocity approaches the freestream velocity at infinity, and that unsteady disturbances radiate away from the airfoil.

2.2. *Flow Decomposition*

For many aeroelastic and aeroacoustic flows of practical interest, the unsteadiness is small compared to the mean flow. For example, at the onset of flutter, the vibration of the

airfoil is small and so is the resulting unsteady flow. Therefore, the unsteady full potential equation may be linearized to obtain a linear variable coefficient equation for the small unsteady disturbance flow.

For numerical accuracy, it will be convenient to work in a coordinate system that conforms to the motion of the airfoil. Consider the case where the airfoil vibrates harmonically with frequency ω. The usual physical coordinates x, y, t are related to the "strained coordinates" ξ, η, τ by the transformation

$$x(\xi, \eta, \tau) = \xi + f(\xi, \eta)e^{j\omega\tau} \tag{6}$$

$$y(\xi, \eta, \tau) = \eta + g(\xi, \eta)e^{j\omega\tau} \tag{7}$$

$$t(\xi, \eta, \tau) = \tau. \tag{8}$$

Here, the physical and strained coordinate system are the same to zeroth order, but differ from first order in the small perturbation functions f and g. The functions f and g are chosen so that in the strained coordinate system the airfoil appears stationary. Said another way, if the nodes of a computational grid are fixed in the strained coordinate system, then in the physical coordinate system, the grid nodes will deform so as to conform to the motion of the airfoil.

Having defined the coordinate transformation, we now decompose the unsteady velocity potential $\hat{\phi}$ into the sum of two parts: a mean or steady potential Φ and an unsteady disturbance potential ϕ, i.e.,

$$\hat{\phi}(\xi, \eta, \tau) = \Phi(\xi, \eta) + \phi(\xi, \eta)e^{j\omega\tau}, \tag{9}$$

where the unsteady potential ϕ is assumed to be much smaller than the mean flow potential Φ. Note that the perturbation series is carried out in the strained coordinate system. Thus, in the physical coordinate system, unsteadiness will arise from the unsteady velocity potential ϕ and the unsteady deformation of the mean velocity potential Φ.

At first, defining the potential decomposition in the strained coordinate system would seem to complicate unnecessarily the solution of the unsteady flow field. However, the use of strained coordinates eliminates the need to extrapolate the unsteady boundary conditions from the instantaneous position of the airfoil to the mean position of the airfoil as required in fixed grid calculations. These extrapolation terms contain second derivatives of the mean flow potential and are very difficult to evaluate accurately in a numerical scheme, especially near the leading and trailing edges. Furthermore, the use of strained coordinates is physically appealing since, to zeroth order, one would expect that the flow around a displaced airfoil would be the same as the steady flow, but displaced to coincide with the new position of the airfoil. Hall [8] and Hall and Clark [9] have shown that the use of strained coordinates greatly improves the accuracy of time-linearized unsteady flow computations.

Having defined the strained coordinates and the flow decomposition, we now need to define the differential operators ∇ and $\partial/\partial t$ in terms of the strained coordinates. To first order, these may be expressed as

$$\nabla = \begin{pmatrix} \frac{\partial}{\partial x} \\ \frac{\partial}{\partial y} \end{pmatrix} = \begin{bmatrix} 1 - f_\xi & -g_\xi \\ -f_\eta & 1 - g_\eta \end{bmatrix} \begin{pmatrix} \frac{\partial}{\partial \xi} \\ \frac{\partial}{\partial \eta} \end{pmatrix} = \mathbf{J}\nabla' \tag{10}$$

and

$$\frac{\partial}{\partial t} = \frac{\partial}{\partial \tau} - \frac{\partial \mathbf{f}}{\partial \tau} \cdot \nabla', \tag{11}$$

where $\mathbf{f} = (f, g)^{\mathrm{T}}$. Next, we substitute Eqs. (6)–(11) into the nonlinear full potential equation and associated near-field and far-field boundary conditions. Collecting terms of zeroth and first order in ϕ and $\mathbf{f}$ gives the mean flow full potential and the time-linearized full potential equations, respectively.

2.3. *Nonlinear Mean Flow Description*

Retaining zeroth-order terms in the full potential equation gives the mean full potential equation

$$\nabla' \cdot (R \nabla' \Phi) = 0, \tag{12}$$

where R is the mean flow static density given by

$$R = \rho_T \left[1 - \frac{\gamma - 1}{2 C_T^2} \nabla' \Phi^2 \right]^{1/(\gamma - 1)} \tag{13}$$

Equation (13) is recognized as the steady continuity equation.

Similarly, the mean flow airfoil boundary condition is given by

$$\frac{\partial \Phi}{\partial n} = 0 \tag{14}$$

On the wake, (14) applies as well, along with the requirement that the mean pressure jump across the wake be zero,

$$[\![P]\!] = 0, \tag{15}$$

where the mean pressure P is given by

$$P = P_T \left[1 - \frac{\gamma - 1}{2 C_T^2} \nabla' \Phi^2 \right]^{\gamma/(\gamma - 1)} \tag{16}$$

Finally, at the far-field boundary, we require the mass flux through the boundary to be equal to the mass flux produced by the freestream. Therefore, we apply the Neumann condition

$$\frac{\partial \Phi}{\partial n} = \mathbf{V}_\infty \cdot \mathbf{n}, \tag{17}$$

where $\mathbf{V}_\infty$ is the freestream velocity, and $\bar{\mathbf{n}}$ is the unit normal to the far-field boundary.

This completes the specification of the mean flow field. Note that the problem is nonlinear in the unknown potential Φ. In practice, the nonlinear problem may be reduced to a sequence of linear problems using Newton iteration.

2.4. *Small Disturbance Unsteady flow Description*

Having described the mean flow field, we now turn our attention to the specification of the small disturbance unsteady flow field. The first-order terms in the series expansion

of the full potential equation, (1), gives the governing equation for the unknown unsteady perturbation potential ϕ, i.e.

$$\begin{aligned}\nabla' \cdot R\nabla'\phi - \nabla' \cdot \left[\frac{R}{C^2}(\nabla'\Phi^T\nabla'\phi + j\omega\phi)\nabla'\Phi\right] - \frac{R}{C^2}(j\omega\nabla'\Phi^T\nabla'\phi - \omega^2\phi)\\ = -\nabla' \cdot [R(\tilde{\mathbf{J}}\nabla'\Phi + \nabla'\cdot\mathbf{f}\nabla'\Phi)] + j\omega\mathbf{f}\cdot\nabla' R\\ + \nabla' \cdot \left[\frac{R}{C^2}\left(\frac{1}{2}\nabla'\Phi^T\tilde{\mathbf{J}}\nabla'\Phi\nabla'\Phi - j\omega\nabla'\cdot\mathbf{f}\nabla'\Phi\nabla'\Phi\right)\right]\\ + \frac{R}{C^2}\left[\frac{j\omega}{2}\nabla'\Phi^T\tilde{\mathbf{J}}\nabla'\Phi + \omega^2\mathbf{f}\cdot\nabla'\Phi\right], \qquad (18)\end{aligned}$$

where $\tilde{\mathbf{J}}$ is the first-order part of $\mathbf{J}^T\mathbf{J} - \mathbf{I}$ and C is local mean flow speed of sound. In (18), we have grouped the terms involving the unknown perturbation potential ϕ on the left, and the terms involving the prescribed deformation of the physical coordinates on the right. Note that the linearized full potential equation, (18), is linear in the unknown perturbation potential ϕ, with variable coefficients that depend upon the mean flow. The right-hand side represents an inhomogeneous forcing term that arises from the motion of the airfoil (and hence unsteady coordinate straining).

Similarly, we find that the linearized boundary conditions on the airfoil surface are given by

$$\frac{\partial\phi}{\partial n} = j\omega\mathbf{f}\cdot\bar{\mathbf{n}} - \tilde{\mathbf{J}}\nabla\Phi\cdot\bar{\mathbf{n}}, \qquad (19)$$

where $\bar{\mathbf{n}}$ is the unit normal to the mean location of the airfoil surface. The first term on the right-hand side of (19) represents the upwash due to the local airfoil velocity normal to the mean position of the airfoil surface. The second term represents an additional upwash required to counteract a downwash resulting from shearing of the mean potential field near the airfoil due to the strained coordinate transformation. Finally, the usual upwash due to rotation of the airfoil does not appear, nor is it required, since the mean potential field in the vicinity of the airfoil rotates with the airfoil.

On the wake, a no-through-flow condition similar to (19) holds, i.e.,

$$\frac{\partial\phi}{\partial n} = j\omega\mathbf{f}\cdot\bar{\mathbf{n}} - \tilde{\mathbf{J}}\nabla\Phi\cdot\bar{\mathbf{n}} + j\omega r_w + V\frac{\partial r_w}{\partial s}, \qquad (20)$$

where r_w is the displacement of the wake normal to its mean position. Note, however, the two additional terms that appear on the right-hand side of (20). These terms appear because motion of the wake, which is not known *a priori*, does not exactly coincide with the motion of the physical coordinates x, y, t corresponding to the mean wake location in ξ, η, τ space. These two terms represent an additional wash due to the translation and rotation of the wake, respectively. Also, the jump in the perturbation pressure across the wake must be zero, so that

$$[\![p]\!] = 0, \qquad (21)$$

where p is the perturbation pressure.

Finally, boundary conditions must be applied on the far-field boundary to ensure that unsteady disturbances propagate away from the airfoil. We apply boundary conditions similar to those proposed by Bayliss and Turkel [29]. In the far field, the mean flow is

uniform and the linearized potential equations may be expressed as

$$-\omega^2\phi + 2j\omega U_\infty \frac{\partial\phi}{\partial\xi} - \left(C_\infty^2 - U_\infty^2\right)\frac{\partial^2\phi}{\partial\xi^2} - C_\infty^2\frac{\partial^2\phi}{\partial\eta^2} = 0, \tag{22}$$

where for simplicity we have assumed that the physical and strained coordinate systems coincide in the far field and that the freestream flow is in the ξ-direction. Here, U_∞ and C_∞ are the freestream flow velocity and speed of sound. For subsonic flows, Bayliss and Turkel [29] have shown that an approximate but accurate radiation boundary condition for the convective wave equation, (22), is given by

$$B_2\phi = \left(C_1 j\omega + \frac{R}{d}\frac{\partial}{\partial R} + \frac{5}{2d}\right)\left(C_1 j\omega + \frac{R}{d}\frac{\partial}{\partial R} + \frac{1}{2d}\right)\phi = 0, \tag{23}$$

where

$$R = (\xi^2 + \eta^2)^{1/2},$$
$$d = \left(\frac{\xi^2}{1 - M_\infty^2} + \eta^2\right)^{1/2},$$

and

$$C_1 = \frac{\left[1 - M_\infty^2\right]^{-1/2}}{C_\infty}\left[1 - \frac{x}{d}\frac{M_\infty}{\left(1 - M_\infty^2\right)^{1/2}}\right].$$

Grouping terms in (23) by powers of ω gives

$$B_2\phi = \frac{1}{d^2}\left(R^2\frac{\partial^2\phi}{\partial R^2} + 3R\frac{\partial\phi}{\partial R} + \frac{\phi}{2}\right) + j\omega\frac{2C_1}{d}\left(R\frac{\partial\phi}{\partial R} + \phi\right) - \omega^2 C_1^2\phi = 0. \tag{24}$$

We have found that for moderate to high reduced frequencies, these boundary conditions are highly nonreflective. However, in the limit of zero reduced frequency, (24) reduces to

$$B_2\phi = 0 = \frac{1}{d^2}\left(R^2\frac{\partial^2\phi}{\partial R^2} + 3R\frac{\partial\phi}{\partial R} + \frac{\phi}{2}\right). \tag{25}$$

The third term on the right-hand side is inconsistent with the linearization of the mean flow far-field boundary condition. For instance, at very low reduced frequencies, the unsteady lift due to a pitching motion of the airfoil with unit amplitude should be equal to the lift curve slope. However, if the term $\phi/2d^2$ is retained in the far-field boundary condition, the correct lift is not obtained. Therefore, (24) is used at the far-field boundary, but with the term $\phi/2d^2$ omitted. We have found that this modification greatly improves the very low-frequency calculations and does not significantly alter the moderate and high-frequency behavior.

This completes the specification of the small disturbance unsteady flow problem. Once this linear boundary value problem has been solved, the unsteady perturbation pressure on the surface of the airfoil may be found using the linearized Bernoulli equation,

$$p = -R\left[\nabla'\Phi^T\nabla'\phi + j\omega\phi - j\omega\mathbf{f}\cdot\nabla'\Phi + \frac{1}{2}\nabla'\Phi^T\tilde{\mathbf{J}}\nabla'\Phi\right]. \tag{26}$$

The unsteady pressure can then be integrated to find the unsteady lift and moment.

2.5. *Discretization of the Governing Equations*

Solving for the unsteady perturbation flow is a two-step process. First, the equations governing the nonlinear mean flow field are discretized on a computational grid and solved numerically. Then, the mean flow solution is used to form the variable coefficients appearing in the small disturbance equations, which are also solved numerically for each vibratory mode and frequency of interest.

Hall [8] has shown that both the mean flow and linearized unsteady potential equations are the Euler–Lagrange equations of variational principles that are extensions of a variational principle given by Bateman [30]. Furthermore, the mean flow and linearized unsteady airfoil boundary conditions are identical to the natural boundary conditions of the variational principles. Therefore, in the present work, we discretize the field equations and the airfoil boundary conditions using variational finite elements. The elements are four-node isoparametric elements. The far-field boundary conditions and the wake boundary conditions are discretized using a combination of finite element and finite difference techniques.

The discretized equations for the mean flow (12) are nonlinear and are solved using Newton iteration. The discretized equations governing the unsteady perturbation flow (18) are, of course, linear and of the form

$$\mathbf{A}\phi = \mathbf{b}, \tag{27}$$

where ϕ is the vector containing the unknown values of velocity potential ϕ at each of the grid nodes and the unknown wake motion r_w at each node along the wake. The matrix $\mathbf{A}$ is a large, sparse, complex, nonsymmetric matrix. The vector $\mathbf{b}$ arises from the prescribed motion of the airfoil (and, hence, the physical coordinate system). Using the conventional "direct" time-linearized solution technique, one would solve (27) by Gaussian elimination or LU decomposition for each frequency and mode shape of vibration. In Section 3, we describe an alternative modal analysis technique based on the eigenmodes of the fluid dynamic system.

3. REDUCED-ORDER MODELLING TECHNIQUE

3.1. *Normal Mode Analysis*

Consider the assembled matrix equation for the unsteady small disturbance flow, (27). Every term in the matrix $\mathbf{A}$ is quadratic in the frequency ω so that

$$\left(\mathbf{A}_0 + j\omega\mathbf{A}_1 + \omega^2\mathbf{A}_2\right)\phi = \mathbf{b}, \tag{28}$$

where the matrices $\mathbf{A}_0$, $\mathbf{A}_1$, and $\mathbf{A}_2$ are real nonsymmetric $n \times n$ matrices and where n is the number of unknown entries in ϕ. (We remark, however, that without the wake and far-field boundary conditions, the matrices $\mathbf{A}_0$ and $\mathbf{A}_2$ would be symmetric and the matrix $\mathbf{A}_1$ would be skew symmetric.) The form of discretized equations is similar in form to that obtained for linear structural dynamic problems. As in structural dynamics, it will prove useful to solve (28) using a normal mode analysis. Toward that end, it will be convenient to convert (28) to first-order form. Let $\mathbf{\Phi}$ be the "state" of the system defined by

$$\mathbf{\Phi} = \begin{Bmatrix} j\omega\phi \\ \phi \end{Bmatrix}. \tag{29}$$

Equation (28) may then be expressed as

$$\mathcal{A}\mathbf{\Phi} - j\omega\mathcal{B}\mathbf{\Phi} = \bar{\mathbf{b}}, \tag{30}$$

where

$$\mathcal{A} = \begin{bmatrix} \mathbf{G} & 0 \\ \mathbf{A}_1 & \mathbf{A}_0 \end{bmatrix}, \quad \mathcal{B} = \begin{bmatrix} 0 & \mathbf{G} \\ \mathbf{A}_2 & 0 \end{bmatrix}, \quad \bar{\mathbf{b}} = \begin{Bmatrix} 0 \\ \mathbf{b} \end{Bmatrix},$$

and where $\mathbf{G}$ is any nonsingular matrix.

Next, we seek to diagonalise (30). Therefore, we need to compute the left and right eigenvectors of the generalized eigenvalue problem

$$\mathcal{A}\mathbf{x}_i = \lambda_i \mathcal{B}\mathbf{x}_i, \tag{31}$$

where λ_i is the ith eigenvalue and $\mathbf{x}_i$ is the corresponding right eigenvector. (For convenience, we order the eigenvalues from smallest to largest in magnitude.) More generally, we may write

$$\mathcal{A}\mathbf{X} = \mathcal{B}\mathbf{X}\mathbf{\Lambda}, \tag{32}$$

where $\mathbf{X}$ is a $2n \times 2n$ matrix whose i-th column is the eigenvector corresponding to λ_i, and $\mathbf{\Lambda}$ is a diagonal matrix whose ith diagonal entry is the eigenvalue λ_i. Similarly, the generalized left eigenvector problem may be written as

$$\mathcal{A}^{\mathrm{T}}\mathbf{Y} = \mathcal{B}^{\mathrm{T}}\mathbf{Y}\mathbf{\Lambda}, \tag{33}$$

where $\mathbf{Y}$ is a square matrix containing the $2n$ left eigenvectors $\mathbf{y}_i$. The left and right eigenvectors are orthogonal with respect to the matrices $\mathcal{A}$ and $\mathcal{B}$; we normalize the eigenvectors so that they are orthonormal with respect to $\mathcal{B}$. Therefore,

$$\mathbf{Y}^{\mathrm{T}}\mathcal{B}\mathbf{X} = \mathbf{I} \tag{34}$$

and

$$\mathbf{Y}^{\mathrm{T}}\mathcal{A}\mathbf{X} = \mathbf{\Lambda}. \tag{35}$$

3.2. *Standard Reduced-Order Model*

Next, we let the state vector $\mathbf{\Phi}$ be a linear combination of the right eigenvectors, i.e.,

$$\mathbf{\Phi}e^{j\omega\tau} = \mathbf{X}\mathbf{w}e^{j\omega\tau}, \tag{36}$$

where $\mathbf{w}$ is the vector of modal coordinates and where we have temporarily reintroduced $e^{j\omega\tau}$ to emphasize that we seek the unsteady response to harmonic forcing. Substitution of (36) into (30) gives

$$\mathcal{A}\mathbf{X}\mathbf{w} - j\omega\mathcal{B}\mathbf{X}\mathbf{w} = \bar{\mathbf{b}}. \tag{37}$$

Premultiplying (37) by $\mathbf{Y}^{\mathrm{T}}$ and making use of the orthogonality conditions, (34) and (35), gives

$$\lambda_i w_i - j\omega w_i = \delta_i, \quad i = 1, 2n \tag{38}$$

where δ_i is the participation factor given by $\delta_i = \mathbf{y}_i^T \cdot \bar{\mathbf{b}}$. Note that (38) represents a set of uncoupled equations for the unknown modal coordinates, w_i. The amount of each mode present in the solution may be computed independently; the contribution of each mode can then be summed to determine $\mathbf{\Phi}$, so that

$$\mathbf{\Phi} = \sum_{i=1}^{2n} w_i \mathbf{x}_i = \sum_{i=1}^{2n} \frac{\delta_i}{\lambda_i - j\omega} \mathbf{x}_i. \tag{39}$$

Note that the amount of each mode present in the solution is just the participation factor δ_i divided by the difference between the eigenvalue λ_i and the forcing frequency $j\omega$. Thus, modes with eigenfrequencies much larger than the forcing frequency are not strongly excited. Hence, as is commonly done in structural dynamic problems, we truncate the series in (39) at $i = m$, where $m < 2n$ and $|\lambda_m| \gg |\omega|$.

3.3. *Static Correction Technique*

One finds that when using the standard reduced order model (mode superposition) described in Section 3.2, an excessively large number of eigenmodes must sometimes be retained to obtain accurate results. The problem is that while the dominant eigenmodes have been retained, all of the eigenmodes participate in the response to some degree. However, if the frequency of the excitation is well separated from the eigenfrequency of a given mode, then that mode will respond in an essentially static way. This suggests that the unsteady solution $\mathbf{\Phi}$ may be divided into two parts, i.e.,

$$\mathbf{\Phi} = \mathbf{\Phi}^{(1)}_{\text{static}} + \tilde{\mathbf{\Phi}}. \tag{40}$$

The first term on the right-hand side of (40) is the solution one would obtain if the excitation were quasi-steady and is found by solving the linear system of equations

$$\mathcal{A}\mathbf{\Phi}^{(1)}_{\text{static}} = \bar{\mathbf{b}}. \tag{41}$$

The second term on the right-hand side of (40) is a correction that accounts for the fact that those eigenmodes with small eigenfrequencies respond dynamically.

Next, we let $\tilde{\mathbf{\Phi}} = \mathbf{X}\tilde{\mathbf{w}}$. Substitution of this expression and (40) into (30), and again, making use of the orthogonality conditions, gives after some manipulation

$$\mathbf{\Phi} = \sum_{i=1}^{2n} \frac{j\omega}{\lambda_i} \frac{\delta_i}{\lambda_i - j\omega} \mathbf{x}_i + \mathbf{\Phi}^{(1)}_{\text{static}}. \tag{42}$$

The advantage of (42) over (39) is that the series in (42) converges more rapidly since $|j\omega/\lambda_i| \ll 1$ for large i. Thus, many fewer terms need to be retained in the series to obtain accurate results. This technique is completely analogous to the "static correction" or "mode acceleration" methods used in structural dynamics problems (see, e.g. [31]).

Another way to derive (42) is to note that

$$\frac{1}{\lambda_i - j\omega} = \frac{j\omega}{\lambda_i}\frac{1}{\lambda_i - j\omega} + \frac{1}{\lambda_i}. \tag{43}$$

Substitution of (43) into (39) gives

$$\mathbf{\Phi} = \sum_{i=1}^{2n} \frac{j\omega}{\lambda_i}\frac{\delta_i}{\lambda_i - j\omega}\mathbf{x}_i + \sum_{i=1}^{2n} \frac{\delta_i}{\lambda_i}\mathbf{x}_i. \tag{44}$$

The second series on the right is recognized as the static response $\mathbf{\Phi}^{(1)}_{\text{static}}$. This process can be repeated again so that

$$\mathbf{\Phi} = \sum_{i=1}^{2n} \left(\frac{j\omega}{\lambda_i}\right)^2 \frac{\delta_i}{\lambda_i - j\omega}\mathbf{x}_i + \sum_{i=1}^{2n} j\omega\frac{\delta_i}{\lambda_i^2}\mathbf{x}_i + \sum_{i=1}^{2n} \frac{\delta_i}{\lambda_i}\mathbf{x}_i. \tag{45}$$

The second term on the right is equal to $\mathbf{\Phi}^{(2)}_{\text{static}}$, where $\mathbf{\Phi}^{(2)}_{\text{static}}$ is the solution to

$$\mathcal{A}\mathbf{\Phi}^{(2)}_{\text{static}} = \mathcal{B}\mathbf{\Phi}^{(1)}_{\text{static}}. \tag{46}$$

Generalized for the case of N_c static corrections, we obtain

$$\mathbf{\Phi} = \sum_{i=1}^{2n} \left(\frac{j\omega}{\lambda_i}\right)^{N_c} \frac{\delta_i}{\lambda_i - j\omega}\mathbf{x}_i + \sum_{k=1}^{N_c} (j\omega)^{k-1}\mathbf{\Phi}^{(k)}_{\text{static}}, \tag{47}$$

where

$$\mathcal{A}\mathbf{\Phi}^{(k)}_{\text{static}} = \mathcal{B}\mathbf{\Phi}^{(k-1)}_{\text{static}}. \tag{48}$$

One might expect that the solution of the linear system of equations given in (48) would make the "method of multiple static corrections" prohibitively expensive. However, the matrix $\mathcal{A}$ need only be factored once using LU decomposition. Thereafter, back substitution is used to solve (48). Furthermore, the matrix $\mathcal{A}$ is factored during the solution of the eigenvalue problem and may be stored for this purpose. Note that the right-hand side of Eq. (28) can be written as a quadratic function of the frequency, that is,

$$\mathbf{b} = \mathbf{b}_0 + j\omega\mathbf{b}_1 + \omega^2\mathbf{b}_2, \tag{49}$$

where the vectors $\mathbf{b}_0$, $\mathbf{b}_1$, and $\mathbf{b}_2$ do not depend on the frequency. Hence, for each type of external excitation (pitch, plunge, or a more general shape deformation), the multiple static corrections can be computed with three back solves and the results used for any frequency of excitation. Note that the eigenvalues and eigenvectors do not depend on the external excitation.

Generally, the first series in (48) converges much more quickly than the standard reduced order model series because for large i, $|j\omega/\lambda_i| \ll 1$. Nevertheless, the method may break down if N_c is too large. This is because the leading order terms in each of the two series in (48) grow rapidly with increasing N_c. The sum of the two series, however, is order unity. In

finite precision arithmetic, such operations can lead to significant roundoff errors. We have found that good results are generally obtained for values of N_c between one and six.

For the reduced-order modelling techniques described above to be computationally viable, one must be able to calculate efficiently all of the eigenvalues and corresponding left and right eigenvectors for which $|\lambda_i| \leq \lambda_{\text{specified}}$, where $\lambda_{\text{specified}}$ is larger than the maximum frequency of interest. The authors have implemented a large, sparse, nonsymmetric, quadratic, generalized eigenvalue solver based on the Lanczos algorithm with reorthogonalisation to solve the eigenvalue problem given by (33) and (34). The interested reader is referred to [32, 33] for a general discussion of the Lanczos algorithm, and to [23] for specific implementation details.

3.4. *Aerodynamic Response to Arbitrary Airfoil Motion*

In this section, we consider the aerodynamic response of an airfoil to arbitrary motion of the airfoil. In the time domain, the state vector $\mathbf{\Phi}(t)$ is described by $2n$ first-order ordinary differential equations of the form

$$\mathcal{A}\mathbf{\Phi}(t) - \mathcal{B}\dot{\mathbf{\Phi}}(t) = \bar{\mathbf{b}}(t) \tag{50}$$

Consider the case of airfoil which is initially at rest that begins to translate downward with amplitude $h(t)$ at time $t = 0$. Taking the Laplace transform of (50) gives

$$\mathcal{A}\mathbf{\Phi}^*(s) - \mathcal{B}\mathbf{\Phi}^*(s) = h^*(s)\left(\mathbf{d}_0 + s\mathbf{d}_1 + s^2\mathbf{d}_2\right), \tag{51}$$

where the superscript " * " denotes that Laplace transform of the quantity in question. The vectors $\mathbf{d}_0$, $\mathbf{d}_1$, and $\mathbf{d}_2$ are constant vectors that depend on the type of airfoil motion. (More precisely, the vectors depend on the details of the prescribed grid motion. For rigid-body grid motion, the vector $\mathbf{d}_0$ is uniform, constant in space, and reduces to zero in the region where the grid pitches with the airfoil.)

Next, we represent the unsteady response $\mathbf{\Phi}(t)$ as a sum of eigenmodes,

$$\mathbf{\Phi}(t) = \sum_{i=1}^{2n} w_i(t)\mathbf{x}_i, \tag{52}$$

where here $w_i(t)$ is the time history of the amplitude of the ith eigenvector. Taking the Laplace transform of (52) gives

$$\mathbf{\Phi}^*(s) = \sum_{i=1}^{2n} w_i^*(s)\mathbf{x}_i. \tag{53}$$

Premultiplying (53) by $\mathbf{y}_j^{\mathrm{T}}$, and making use of the orthogonality properties of the eigenvectors, we find that

$$w_i^*(s) = -h^*(s)\frac{\delta_{0,i} + s\delta_{1,i} + s^2\delta_{2,i}}{s - \lambda_i}, \tag{54}$$

where, for example, $\delta_{0,i} = \mathbf{y}_i^{\mathrm{T}} \cdot \mathbf{d}_0$. Finally, taking the inverse Laplace transform of (54), we find that

$$w_i(t) = \mathcal{L}^{-1}[w_i^*(s)]. \tag{55}$$

As an example, consider the case of an airfoil that is initially at rest that begins to translate with constant speed H_1 at time $t = 0$,

$$h(t) = \begin{cases} H_1 t, & t \geq 0, \\ 0, & t < 0. \end{cases} \tag{56}$$

The Laplace transform of $h(t)$ is given by

$$h^*(s) = H_1/s^2. \tag{57}$$

Substitution of (57) into (54) and (55) gives

$$\mathbf{\Phi}(t) = H_1 \sum_{i=1}^{2n} \left[\left(\frac{t}{\lambda_i} + \frac{1}{\lambda_i^2} \right) \delta_{0,i} + \frac{\delta_{1,i}}{\lambda_i} \right] \mathbf{x}_i - H_1 \sum_{i=1}^{2n} \left(\frac{\delta_{0,i}}{\lambda_i^2} + \frac{\delta_{1,i}}{\lambda_i} + \delta_{2,i} \right) e^{\lambda_i t} \mathbf{x}_i. \tag{58}$$

The first series in (58) is just the "steady-state" response and can easily be shown to be given by

$$\mathbf{\Phi}_{\mathrm{SS}}(t) = H_1 \mathcal{A}^{-1} \left(\mathbf{d}_0 t + \mathbf{d}_1 + \mathcal{B} \mathcal{A}^{-1} \mathbf{d}_0 \right). \tag{59}$$

Finally, the second series is truncated to m terms, where $m \ll 2n$, so that

$$\mathbf{\Phi}(t) = \mathbf{\Phi}_{\mathrm{SS}}(t) - H_1 \sum_{i=1}^{m} \left(\frac{\delta_{0,i}}{\lambda_i^2} + \frac{\delta_{1,i}}{\lambda_i} + \delta_{2,i} \right) e^{\lambda_i t} \mathbf{x}_i. \tag{60}$$

4. COMPUTATIONAL RESULTS

In this section, we use the techniques described in Sections 2 and 3 this paper to compute the steady and unsteady subsonic flow about an isolated NACA 2410 four-digit airfoil. The computational grids used in all cases considered in this paper are O-grids (see Fig. 2). Two

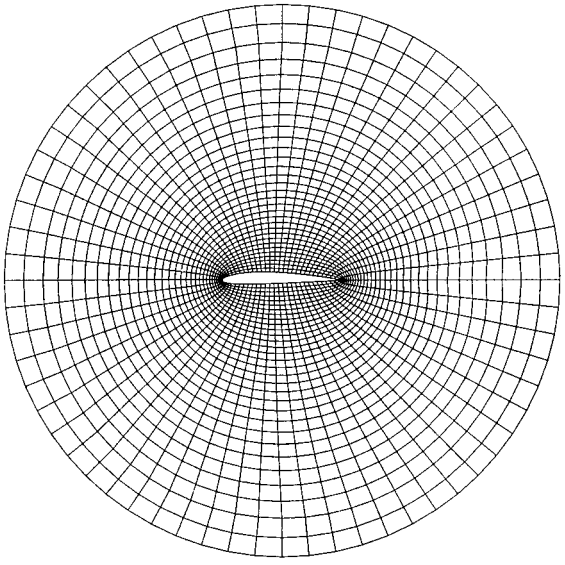

FIG. 2. Typical O-grid used for the computation of flow about an isolated airfoil.

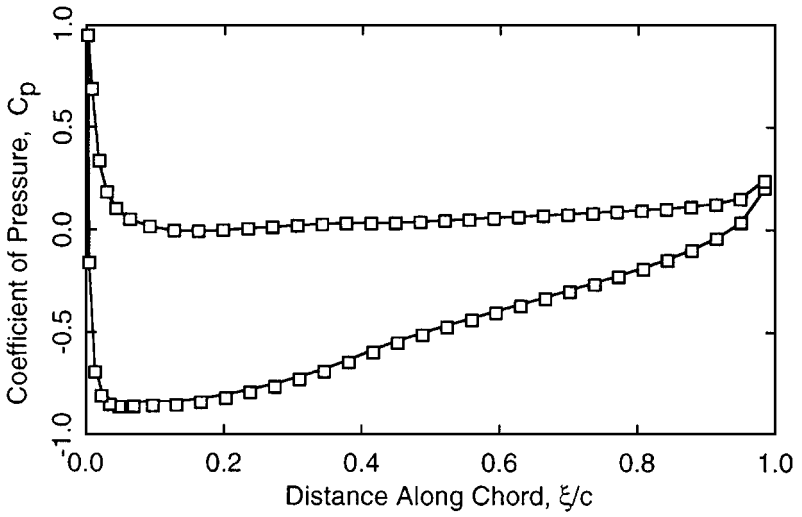

FIG. 3. Steady pressure on surface of NACA 2410 airfoil at 2° angle of attack and a freestream Mach number M_∞ of 0.5: □, 65 × 32 node grid; ———, 65 × 55 node grid.

different O-grids were used: a "small radius" grid with a radius of about 2.35 chords with 65 × 32 mesh points (65 nodes around the airfoil and 32 nodes in the radial direction), and a "large radius" grid with a radius of 6.0 chords with 65 × 55 mesh points. Note that the inner portion of the large radius grid is identical to the small radius grid. The goal of using computational grids with different radii is to demonstrate the effectiveness of the second-order nonreflecting boundary conditions and to determine the influence of changing the size of the computational domain on the eigenfrequencies and eigenmodes of the unsteady flow.

4.1. *Steady Flow Analysis*

To begin, we computed the steady flow about the NACA 2410 airfoil for the case where the freestream Mach number M_∞ is 0.5 and the angle of attack is 2°. As shown in Fig. 3, the steady flow is entirely subsonic for these conditions with a maximum Mach number M of about 0.72 on the suction surface. The results shown in Fig. 3 were computed using two different O-grids: the large radius grid (65 × 55 nodes) and the small radius grid (65 × 32 nodes). The two calculations are in fairly good agreement indicating that, at least for steady flow calculations, the small radius grid has a sufficiently large radius to prevent spurious influences from the far-field boundary. Similar numerical experiments (not presented here) indicate that the resolution of the computational grids is such that the computed steady flow results are essentially grid converged.

4.2. *Direct Time-Linearized Unsteady Flow Analysis*

Next, we consider the unsteady small disturbance flow about the NACA 2410 airfoil for the case where the airfoil vibrates in pitch about its midchord with pitching amplitude α. The unsteady flow is computed using two complementary techniques. In this section, we compute the unsteady flow using the more conventional direct time-linearized approach. In Sections 4.2–4.4 we analyze the unsteady flow using the reduced order modelling techniques described in Section 3.

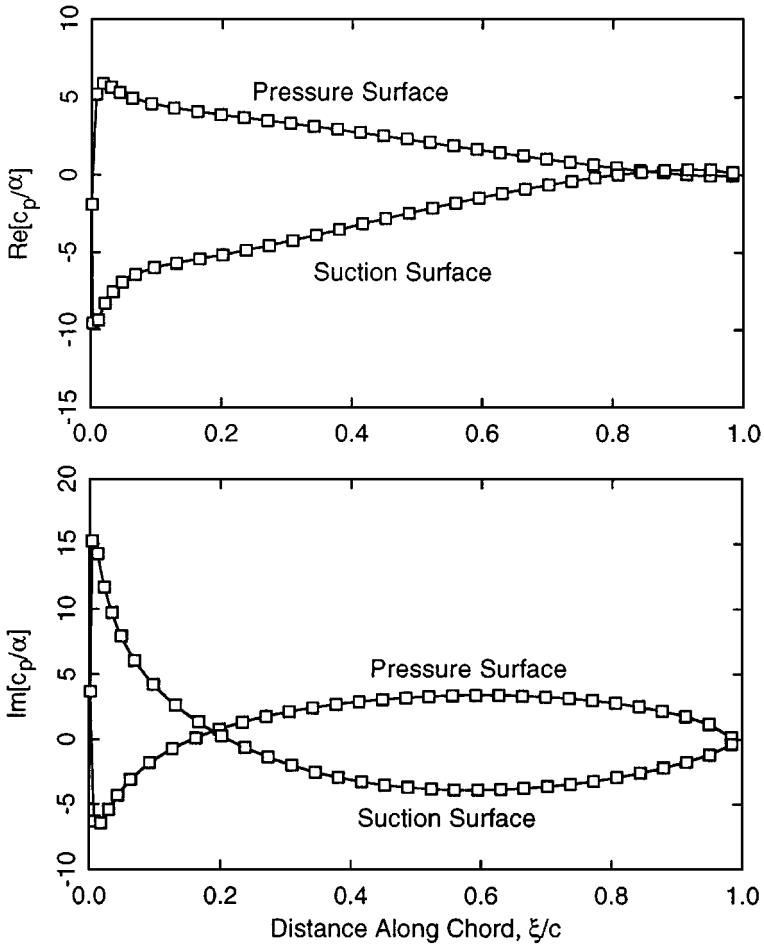

FIG. 4. Unsteady pressure on surface of NACA 2410 airfoil pitching about its midchord with a reduced frequency $\bar{\omega}$ of 2.0: □, 65 × 32 node grid; ———, 65 × 55 node grid.

Consider the case where the airfoil vibrates in pitch about its midchord with a reduced frequency ($\bar{\omega} = \omega c / U_\infty$) of 2.0. Figure 4 shows the real and imaginary parts of the unsteady pressure distribution on the surface of the airfoil. These results were computed using two different O-grids (small and large radius grids). Note that the two computed solutions are virtually indistinguishable, indicating that the nonreflecting boundary conditions allow outgoing pressure waves in the field and shed vorticity in the wake to pass through the far-field boundary with very little reflection. If outgoing waves were reflected, then some of the reflected pressure waves would impinge on the airfoil surface and modify the pressure distribution. These reflected waves would have different phases for the two different grids, and thus the solutions computed on the two different grids would differ one from the other.

Once the unsteady surface pressure has been computed, one can integrate it to obtain the unsteady forces acting on the airfoil. Shown in Fig. 5 is the unsteady lift due to pitching motion of the airfoil for a range of reduced frequencies. Note that the computed lift is insensitive to the location of the computational far-field boundary. We conclude that a computational grid with a radius of 2.35, along with the second-order nonreflecting boundary conditions described in Section 2.4, produce satisfactory computational results for unsteady

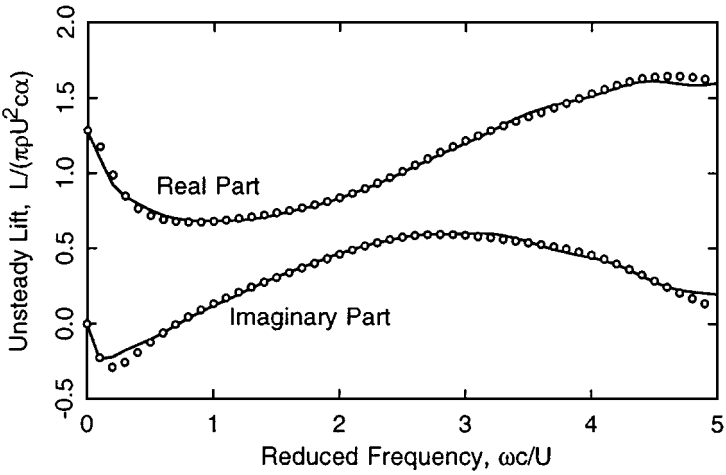

FIG. 5. Unsteady lift on NACA 2410 airfoil pitching about its midchord: ○, 65×32 node grid; ———, 65×55 node grid.

flows with reduced frequencies less than or equal to about 4.5. Similarly, numerical studies show that the solutions are essentially grid converged for this range of reduced frequencies. Note that at zero-reduced frequency, the unsteady lift is purely real as expected with a coefficient of lift $C_{L_\alpha} = 1.28 \times 2\pi$. The real part of the lift is slightly larger than the lift curve slope of a flat-plate airfoil at a Mach number of 0.5 ($C_{L_\alpha} = 1.155 \times 2\pi$) due to thickness and steady loading effects (see, e.g. [34]).

4.3. *Eigenvalues and Eigenmodes of the Unsteady Flow Field*

Next, we computed the eigenfrequencies and eigenmodes of the unsteady flow about the NACA 2410 airfoil. Shown in Fig. 6 are the computed eigenvalues of the flow for a free-stream Mach number M_∞ of 0.5 and an angle attack of 2° for the two different computational grids. In both cases, the eigenvalues are modally dense; that is, the eigenvalues tend to be very closely spaced, forming lines of eigenvalues that emanate from the origin. The authors believe that these lines of eigenvalues correspond to discrete representations of branch cuts. The existence of branch cuts in aerodynamic response functions is well known and indicates that the impulse response contains nonexponential behavior. For example, Desmarais [35] has shown that that the Theodorsen function may be represented by a continued fraction approximation. The poles (eigenvalues) of the continued fraction lie along the negative real axis. As more and more terms are added to the continued fraction, the poles of the continued fraction become more densely spaced. Hall [24] calculated the eigenvalues of a vortex lattice model of unsteady incompressible flow and found that the line of eigenvalues representing the branch cut became more densely spaced as the length of the discrete representation of the wake trailing behind the airfoil was increased. Similarly, Fig. 6 shows that the lines of eigenvalues become more dense as the radius of the computational grid is increased.

By way of comparison, Fig. 7 shows the eigenvalues for the case where the flow about the NACA 2410 airfoil is nearly incompressible ($M_\infty = 0.05$). Again we see that the eigenvalues form dense lines (branch cuts) with branch points at the origin. Also, as before, the lines of eigenvalues become more dense as the radius of the computational domain is increased, although the location of the branch cuts change as the Mach number is changed.

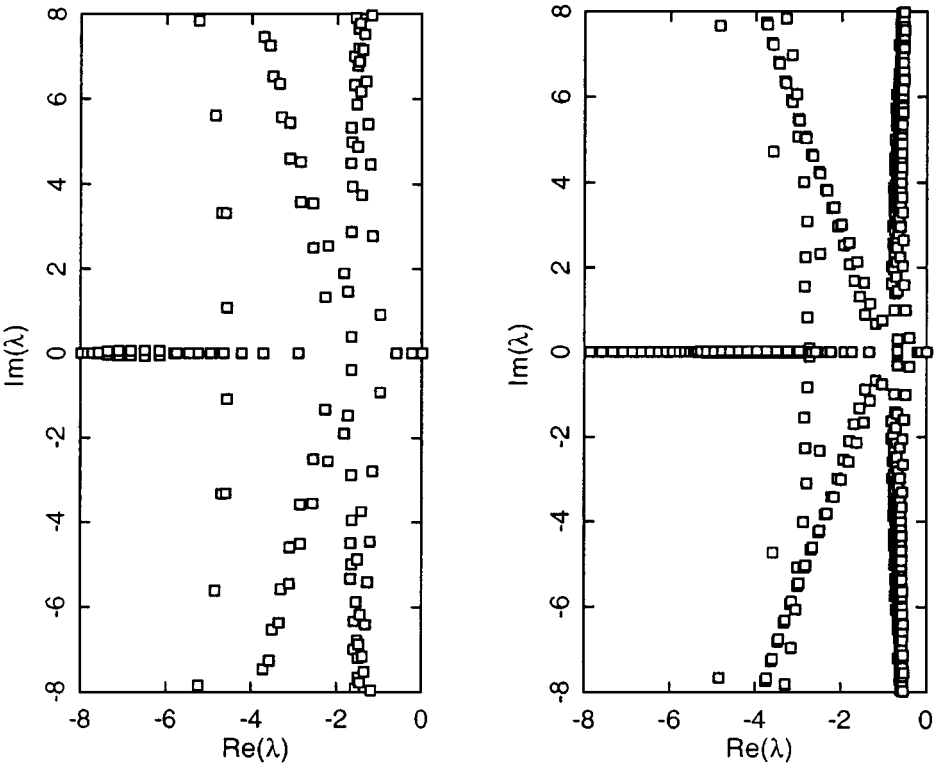

FIG. 6. Eigenvalues of unsteady flow about NACA 2410 airfoil, $M_\infty = 0.5$: left, 65×32 node grid; right, 65×55 node grid.

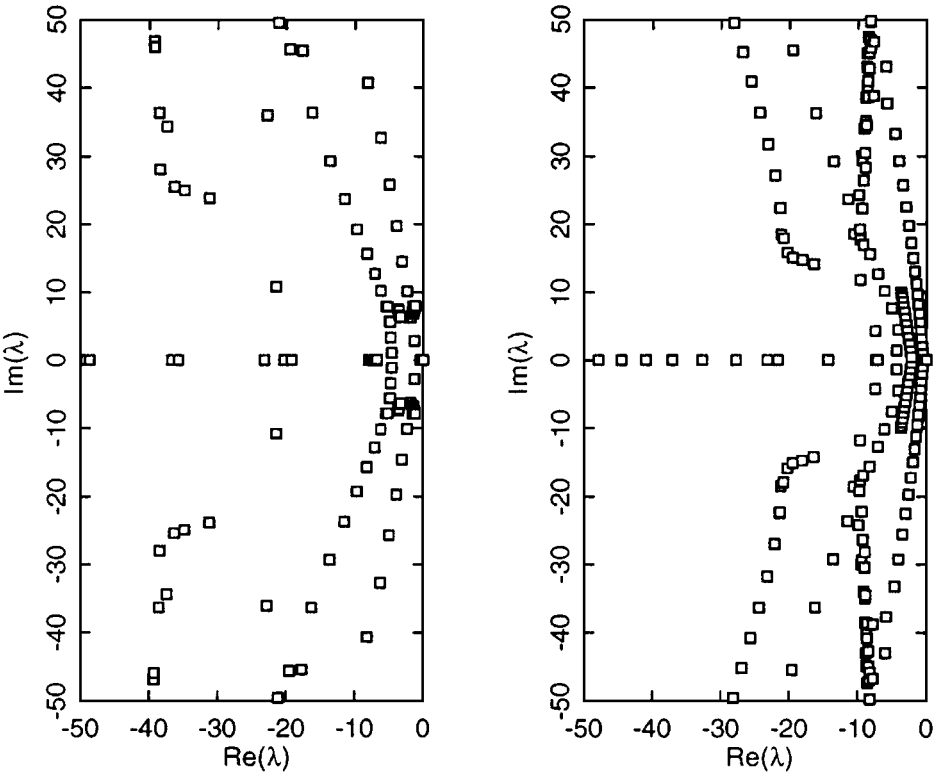

FIG. 7. Eigenvalues of unsteady flow about NACA 2410 airfoil, $M_\infty = 0.05$: left, 65×32 node grid; right, 65×55 node grid.

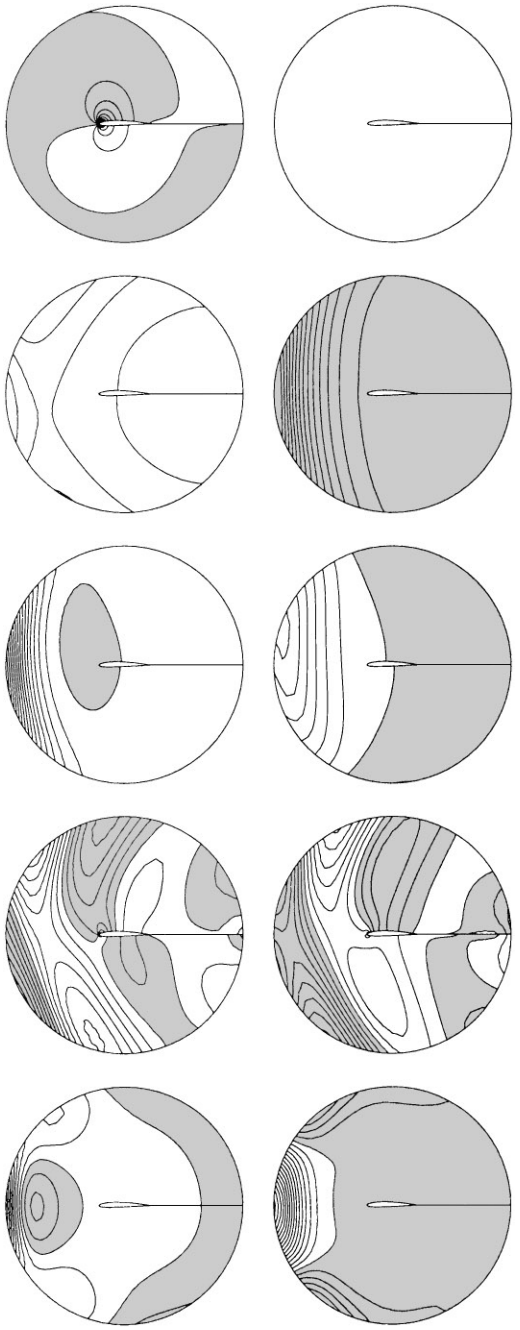

FIG. 8. Contours of unsteady pressure associated with four eigenmodes of flow about NACA 2410 airfoil (65×32 node grid). Top to bottom: mode 2($\lambda = -0.2377 + 0i$), mode 7($\lambda = -1.6582 + 0.3930i$), mode 11($\lambda = -2.2705 + 1.3316i$), mode 15($\lambda = -1.1628 + 2.7910i$), mode 21($\lambda = -2.5529 + 2.5039i$). Left to right: real and imaginary parts. Shading indicates negative values.

Returning to the $M_\infty = 0.5$ case, Fig. 8 shows the contours of unsteady pressure associated with several of the eigenmodes. Note that the pressure waves appear to pass out of the domain without reflection. Shown in Fig. 9 are the pressure distributions on the surface of

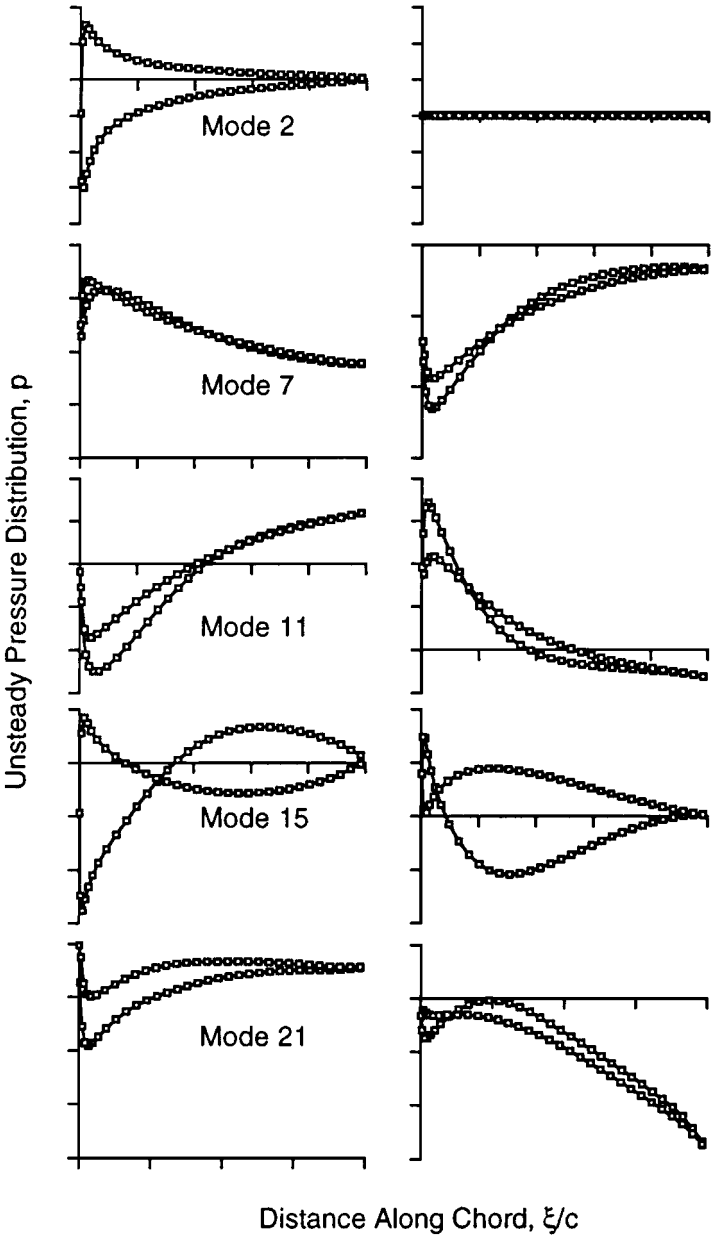

FIG. 9. Unsteady pressure on surface of NACA 2410 airfoil associated with four different eigenmodes. Top to bottom: mode 2, mode 7, mode 11, mode 15, mode 21. Left to right: real and imaginary parts.

the airfoil for each of the eigenmodes shown in Fig. 8. Strictly speaking, the eigenmodes are modes of *potential*, not pressure. The pressure distribution for a particular eigenmode was found by applying the linearized unsteady Bernoulli equation (26) using the corresponding eigenfrequency of that mode. When the eigenmodes are used in the reduced-order model to compute the unsteady response at some other excitation frequency, the pressure distributions associated with these eigenmodes will be different. In fact, the pressure distribution associated with an individual mode at an arbitrary frequency ω will generally not satisfy the

Kutta condition. However, if the contributions from many eigenmodes are retained in the reduced-order model, then the reduced-order model will satisfy the Kutta condition, even if the individual modes in the model do not.

4.4. *Reduced-Order Model Analysis of Unsteady Flow*

Having computed the dominant eigenvalues and eigenmodes of the unsteady flow about the NACA 2410 airfoil, we presently use that information to construct reduced-order models from which the unsteady aerodynamic forces due to airfoil motion may be computed. Using the 22 smallest eigenvalues ($|\lambda| \leq 4.0$) and corresponding eigenvectors (computed on the 65×32 node grid), we constructed a reduced-order model of the unsteady flow due to pitching motion of the airfoil about its midchord. The unsteady pressure distribution on the surface of the pitching airfoil is plotted in Fig. 10 for the case where the airfoils vibrate with a reduced frequency ω of 2.0. Shown is the solution computed using the standard reduced-order model, and the reduced-order model with one and four corrections. Also shown is the solution computed using the direct time-linearized analysis. Note

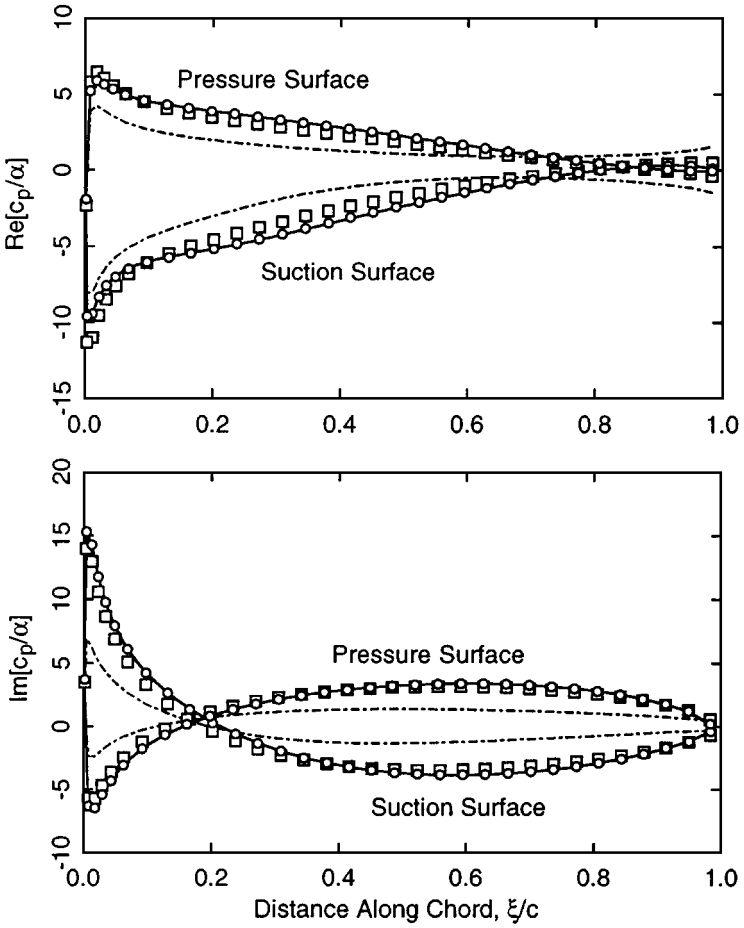

FIG. 10. Unsteady pressure on surface of isolated NACA 2410 airfoil pitching about its midchord with a reduced frequency $\bar{\omega}$ of 2.0: ———, direct time-linearized solution; — - —, 22 eigenmodes; □, 22 eigenmodes plus one correction; ○, 22 eigenmodes plus four corrections.

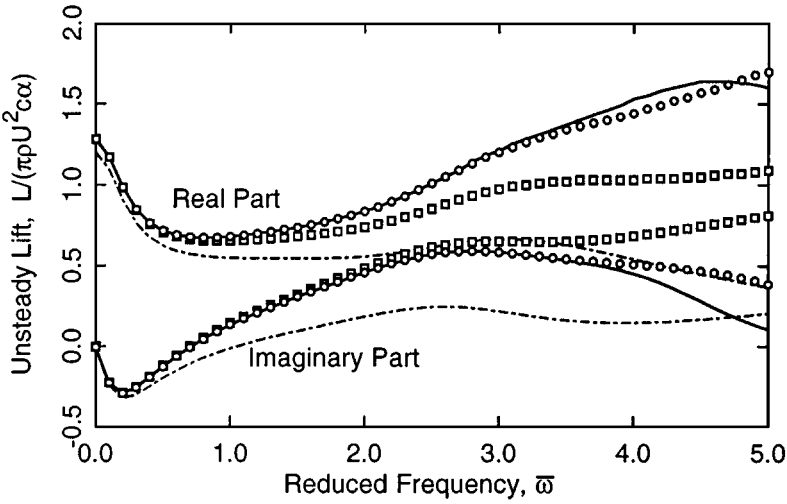

FIG. 11. Unsteady lift on NACA 2410 airfoil pitching about its midchord: ———, direct time-linearized solution; — - —, 22 eigenmodes; □, eigenmodes plus one correction; ○, 22 eigenmodes plus four corrections.

that the results computed using the standard reduced-order model differ greatly from the direct analysis. In particular, one observes that the Kutta condition is not satisfied. With one static correction, the reduced-order model solution is improved significantly. With four static corrections, the results of the direct time-linearized analysis and the reduced-order model are virtually identical. This is especially remarkable considering that 22 eigenmodes correspond to just 0.54% of the total number of eigenmodes for this computational grid.

Next, using the same reduced-order model, we computed the unsteady lift due to pitching motion of the airfoil for a range of reduced frequencies. Shown in Fig. 11 is the unsteady lift predicted using the standard reduced order model, as well as the solution found using the direct time-linearized analysis. While the standard reduced-order model correctly predicts some of the qualitative behavior of the direct time-linearized solution, quantitatively the two solutions differ significantly. Also shown in Fig. 11 are the results of the reduced-order model using a single static correction and four static corrections. Note that with four static corrections, the reduced-order model gives very good results for reduced frequencies $\bar{\omega}$ up to about 3.5 using just 0.54% of the total number of eigenmodes.

We note that for the high reduced frequencies considered in this example, we needed to retain 22 eigenmodes. However, if one is interested in the response at lower frequencies, as would be the case in most aeroelastic problems, then fewer modes would need to be retained in the model. For example, to model the response for reduced frequencies up to unity would require only about seven modes.

Finally, we remark on the computational requirements of the reduced-order model. A single direct time-linearized solution computed using a 65×32 node grid required about 7 s of computer time on a Silicon Graphics Indigo 4400 workstation. To compute the 22 smallest eigenvalues ($|\lambda_i| \leq 4.0$) and the corresponding left and right eigenvectors required just 194 s, about an order of magnitude more than the direct solution. However, once the eigenmodes have been computed, the response over a range of frequencies and mode shapes of vibration can be obtained for almost no additional cost.

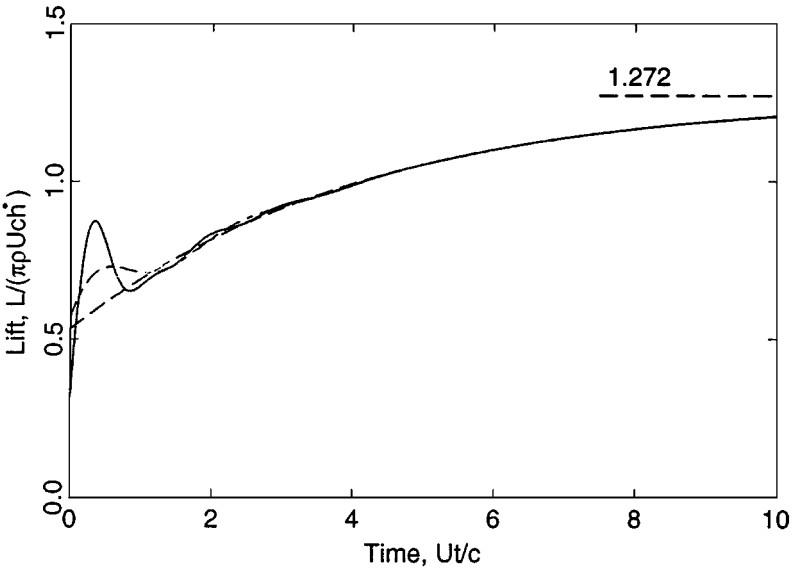

FIG. 12. Indicial lift due to plunging of a NACA 2410 airfoil in subsonic flow. $M_\infty = 0.5$. ———, 2 eigenmodes; —·—, 22 eigenmodes; ———, 110 eigenmodes. Indicial lift due to plunging of a flat plate at $M_\infty = 0.5$: —○—.

4.5. *Indicial Response Computed Using the Reduced Order Model*

Although the main emphasis in this paper has been to compute the aerodynamic response of the airfoil to a harmonic disturbance, one may also use the eigenmode information to compute the response to arbitrary disturbances. Shown in Fig. 12 is the unsteady time history of the lift acting on the airfoil due to a step change in the plunging velocity of the airfoil. These results were computed using 2, 22, or 110 eigenmodes plus a single static correction. For long times, the lift asymptotically approaches 1.272, which as expected is approximately equal to the steady lift curve slope divided by 2π. It would appear from these results that the response for moderate nondimensional times ($Ut/c \geq 5$) can be predicted quite well using just two eigenmodes.[1]

For small to moderate times ($0.2 \leq Ut/c \leq 5.0$), the shape of the lift curve is at least qualitatively correct as more eigenmodes are included in the reduced-order model. For example, the unsteady lift at $t = 0$ can be computed using piston theory. For flat plate airfoils, the initial coefficient of lift should be equal to $2/(\pi M) = 1.27$. The lift should then decrease to a minimum of about 0.7 at a time $Ut/c \approx 0.75$ (see, e.g. [36]). The present results qualitatively agree with the classical results, except for very small times. For very small times, an increasing number of eigenmodes must be retained. However, these eigenmodes have very large eigenfrequencies and, therefore, cannot be accurately computed using computational grids with finite resolution. For this reason, responses at very small times cannot be accurately predicted. This deficiency should not be attributed to the reduced-order model, but rather to truncation errors associated with the original finite element discretization.

[1] The lowest frequency eigenmode has an eigenfrequency of zero, with an eigenmode shape corresponding to a constant potential. This mode does not contribute to the unsteady lift. Therefore, for the results shown in Fig. 12, only the second eigenmode contributes to the unsteady lift.

5. DISCUSSION

In this paper, we have presented an eigenanalysis and reduced-order modelling technique for predicting unsteady flows about isolated airfoils. We have found that complex unsteady flows can be modelled accurately using a small number of eigenmodes. Physically, this is because the unsteady flow may be divided into two parts: a quasi-static portion plus a dynamic part that represents a correction to the quasi-static part. The dynamic portion of the unsteady flow can be further decomposed into a sum of fluid eigenmodes. However, only those eigenmodes with eigenvalues approximately equal to or smaller than the excitation frequency participate significantly. Hence, a very few eigenmodes must be computed. Once the eigenmodes have been computed, the reduced order model may be used to analyze the unsteady aerodynamic response over a wide range of frequencies and mode shapes for very little additional computational effort. Also, the technique may be readily applied to existing time-domain and frequency-domain analyses.

Depending on the range of frequencies of interest and the size of the aerodynamic discretization, the eigenmode-based reduction can be a very efficient and attractive approach. This technique has a number of advantages over more conventional time-marching, time-linearized methods, or even proper orthogonal decomposition techniques. For small to medium size problems, the computation of the eigenmode information required for the reduced-order model is modest, and the eigenmode reduction approach is faster than proper orthogonal decomposition. For large problems, such as three-dimensional flows about wings, the computation of the eigenvectors become increasingly difficult, and proper orthogonal decomposition may be the preferred approach.

We note that the form of the reduced-order model, a low-order rational polynomial in $j\omega$, is ideally suited for use in the design of active control strategies. The poles of the transfer function are the eigenvalues of the fluid system and, hence, are independent of the mode shape of airfoil vibration. The zeros, however, will depend on both the mode shape of airfoil vibration and the desired output force (e.g., the unsteady lift resulting from pitching motion).

Finally, the eigenmode information itself may provide important insights into the physical behavior of unsteady flows. For example, the authors have recently applied this technique to viscous flow models and have been able to predict the onset of flow instabilities, e.g., rotating stall in cascades with fairly large regions of separations [37]. Work is underway to extend the method to transonic flow calculations.

ACKNOWLEDGMENTS

This material is based upon work supported by the National Science Foundation under Grant CTS-9157908. The United States government has certain rights in this material. Additional support was provided by a grant from the Lord Foundation of North Carolina. A preliminary version of this paper was presented at the *ASME International Mechanical Engineering Conference and Exhibition, Chicago, IL, November* 6–11, 1994.

REFERENCES

1. J. T. Batina, *AIAA J.* **29**, 327 (1991).
2. O. O. Bendiksen and K. A. Kousen, Transonic flutter analysis using the Euler equations, AIAA Paper 87-0911 (1987).

3. N. M. Chaderjian and G. P. Guruswamy, *J. Aircraft* **29**, 326 (1992).
4. G. A. Davis and O. O. Bendiksen, *AIAA J.* **31**, 1051 (1993).
5. B. A. Robinson, J. T. Batina, and T. Y. Yang, *AIAA J.* **31**, 1626 (1993).
6. R. D. Rausch, J. T. Batina, and T. Y. Yang, *J. Aircraft* **28**, 781 (1991).
7. F. E. Ehlers and W. H. Weatherill, *J. Aircraft* **28**, 545 (1991).
8. K. C. Hall, *AIAA J.* **31**, 891 (1993).
9. K. C. Hall and W. S. Clark, *AIAA J.* **31**, 540 (1993).
10. K. C. Hall and E. F. Crawley, *AIAA J.* **27**, 777 (1989).
11. D. G. Holmes and H. A. Chuang, 2D Linearized harmonic Euler flow analysis for flutter and forced response, in *Unsteady Aerodynamics, Aeroacoustics, and Aeroelasticity of Turbomachines and Propellers*, edited by H. Atassi (Springer-Verlag, New York, 1993), p. 213.
12. J. M. Verdon and J. R. Caspar, *J. Fluid Mech.* **149**, 403 (1984).
13. D. S. Whitehead and R. J. Grant, Force and moment coefficients of high deflection cascades, in *Proceedings of the 2nd International Symposium on Aeroelasticity in Turbomachines*, edited by P. Suter (Juris-Verlag, Zurich, 1981), p. 85.
14. E. H. Dowell, A simple method for converting frequency domain aerodynamics to the time domain, NASA Tech. Memo 81844 (1980).
15. W. Eversman and A. Tewari, *J. Aircraft* **28**, 545 (1991).
16. W. Eversman and A. Tewari, *J. Aircraft* **28**, 553 (1991).
17. L. D. Peterson and E. F. Crawley, *J. Aircraft* **25**, 121 (1988).
18. R. Parker, *J. Sound Vibration* **5**, 330 (1967).
19. A. Rizzi and L.-E. Eriksson, *J. Fluid Mech.* **148**, 45 (1984).
20. A. J. Mahajan, E. H. Dowell, and D. B. Bliss, *J. Comput. Phys.* **97**, 398 (1991).
21. A. J. Mahajan, E. H. Dowell, and D. B. Bliss, *J. Aircraft* **29**, 555 (1991).
22. A. J. Mahajan, M. A. Bakhle, and E. H. Dowell, An efficient procedure for cascade aeroelastic stability determination using nonlinear, time-marching aerodynamic solvers, AIAA Paper 93-1631 (1993).
23. K. Hall, R. Florea, and P. Lanzkron, *J. Turbomachinery* **117**, 375 (1995). [*Presented at the 39th International Gas Turbine and Aeroengine Congress and Exposition, The Hague, Netherlands, June 13–16, 1994*, ASME Paper 94-GT-291]
24. K. C. Hall, *AIAA J.* **32**, 2426 (1994).
25. M. C. Romanowski and E. H. Dowell, Using eigenmodes to form an efficient Euler based unsteady aerodynamic analysis, in *Aeroelasticity and Fluid Structure Interaction Problems*, edited by P. P. Friedmann and J. C. I. Chang, AD-Vol. 44. (Am. Soc. Mech. Eng., New York, 1994), [Presented at 1994 International Mechanical Engineering Congress and Exposition, Chicago, IL, Nov. 6–11, 1994]
26. M. C. Romanowski, Reduced-order unsteady aerodynamic and aeroelastic models using Karhunen–Loève eigenmodes, AIAA Paper 96-3981 (1996). [Presented at the *6th AIAA/USAF/NASA/ISSMO Symposium on Multidisciplinary Analysis and Optimization, Bellevue, WA, September* 4–6, 1996]
27. L. Sirovich, *Quart. Appl. Math.* **45**, 561 (1987).
28. P. Holmes, H. L. Lumley, and G. Berkooz, *Turbulence, Coherent Structures, Dynamical Systems and Symmetry* (Cambridge Univ. Press, Cambridge, 1996).
29. A. Bayliss and E. Turkel, *J. of Comput. Phys.* **48**, 182 (1982).
30. H. Bateman, *Proc. National Academy of Sciences* **16**, 816 (1930).
31. J. L. Humar, *Dynamics of Structures* (Prentice–Hall, Englewood Cliffs, NJ, 1990).
32. J. Cullum and R. Willoughby, *Lanczos Algorithms for Large Symmetric Eigenvalue Computtations. I. Theory;* Vol. II. *Programs*, Progress in Scientific Computing, Vols. 3 and 4 (Birkhauser, Boston, 1985).
33. Y. Saad, *Numerical Methods for Large Eigenvalue Problems* (Manchester Univ. Press, Manchester, UK, 1992).
34. I. H. Abbot and A. E. von Doenhoff, *Theory of Wing Sections* (Dover, New York, 1959).

35. R. N. Desmarais, A Continued Fraction Representation for Theodorsen's Circulation Function, NASA Tech. Memo 81838, 1980.

36. R. L. Bisplinghoff, H. Ashley, and R. L. Halfman, *Aeroelasticity* (Addison–Wesley, Cambridge, MA, 1955).

37. R. Florea, K. Hall, and P. G. Cizmas, Eigenmode analysis unsteady viscous flows in a turbomachinery cascades, in *Proceedings of the 8th International Symposium on Unsteady Aerodynamics and Aeroelasticity of Turbomachines*, 1997. edited by T. Fransson.